CrossMark

ORIGINAL ARTICLE

# Annexin A2 regulates angiogenesis and invasion phenotypes of malignant glioma

**Manabu Onishi · Tomotsugu Ichikawa · Kazuhiko Kurozumi · Satoshi Inoue ·
Tomoko Maruo · Yoshihiro Otani · Kentaro Fujii · Joji Ishida · Yosuke Shimazu ·
Koichi Yoshida · Hiroyuki Michiue · E. Antonio Chiocca · Isao Date**

**Abstract** We have established a pair of animal models (J3T-1 and J3T-2) with different invasive and angiogenic phenotypes, and demonstrated that annexin A2 is expressed at higher levels in J3T-1 than J3T-2 cells. The function of annexin A2 in relation to angiogenesis and invasion was investigated using these models. Stable silencing or overexpression of annexin A2 in J3T-1 and J3T-2 cells (J3T-1shA and J3T-2A cells) was established and used. Thirty human glioblastoma samples were evaluated for expression of annexin A2, vascular endothelial growth factor (VEGF) and platelet-derived growth factor (PDGF). Immunohistochemical and quantitative reverse-transcription polymerase chain reaction analyses revealed higher expression of annexin A2, VEGF and PDGF in J3T-1 and J3T-2A cells. Cultured J3T-1 and J3T-2A cells exhibited higher adhesive ability to endothelial cells. Histopathological analysis of animal brain tumors revealed that J3T-1 and J3T-2A tumors displayed marked angiogenesis and invasion along the neovasculature, whereas J3T-2 and J3T-1shA tumors exhibited diffuse, infiltrative invasion without angiogenesis. Positive expression of annexin A2 was observed in tumor cells surrounding dilated vessels in 25/30 human glioblastoma specimens. Our results reveal that the phenotype of glioma invasion is closely related to angiogenesis. We identify annexin A2 as a factor regulating angiogenesis and invasion of malignant gliomas.

**Keywords** Angiogenesis · Animal model · Annexin A2 · Glioma · Invasion

## Introduction

Glioblastoma is the most common and lethal form of brain tumor, with a median survival time of 14–15 months. To date, the established therapeutic regimen is surgical resection followed by radiation and temozolomide (TMZ)-based chemotherapy. TMZ, a DNA-alkylating agent, prolongs the survival time of glioblastoma patients for several months [1]. Despite advances in surgical and medical therapy, glioblastoma still remains a fatal disease. The formation of abnormal tumor vasculature and glioma cell invasion, coupled with neovasculature or white matter tracts, is believed to be the major factor underlying the resistance of these tumors to treatment. Therefore, understanding the mechanisms underlying angiogenesis and invasion in glioblastoma is essential for the development of novel, curative therapies. However, glioma angiogenesis and invasion are challenging to study in experimental settings since the majority of animal models fail to mimic the unique angiogenesis and invasiveness of human glioma cells [2, 3].

We have established two novel animal models with different invasive and angiogenic phenotypes [2, 3]. Two subclones, J3T-1 and J3T-2, were established by passaging the parental canine glioma cell line, J3T, in immunocompromised animals. These cells form tumors following intracerebral inoculation in athymic mouse and rat brains. J3T-1 cells clustered around dilated blood vessels at tumor

M. Onishi · T. Ichikawa (✉) · K. Kurozumi · S. Inoue ·
T. Maruo · Y. Otani · K. Fujii · J. Ishida · Y. Shimazu ·
K. Yoshida · H. Michiue · I. Date
Department of Neurological Surgery, Okayama University
Graduate School of Medicine, Dentistry, and Pharmaceutical
Sciences, 2-5-1 Shikatacho, Kitaku, Okayama 700-8558, Japan
e-mail: tomoichi@cc.okayama-u.ac.jp

E. Antonio Chiocca
Department of Neurosurgery, Brigham and Women's/Faulkner
Hospital, 75 Francis Street, Boston, MA 02116, USA

borders, whereas J3T-2 cells exhibited diffuse, single-cell infiltration into surrounding normal parenchyma. Marked angiogenesis was observed only in J3T-1 gliomas. These animal glioma models mimic the two phenotypes of human glioblastoma invasion: angiogenesis-dependent and angiogenesis-independent invasion. Our models can be readily established without complicated cell preparation, and provide a reproducible model of tumor development with the same phenotypic growth as that observed in human glioma [2].

Proteomic analysis of invasion-related proteins using these invasive glioma cell lines was previously reported [4]. These studies identified increased expression of four proteins in J3T-1 cells and 14 proteins in J3T-2 cells, using liquid chromatography–mass spectrometry analysis (LC–MS/MS). One of these candidate proteins, annexin A2, was expressed at higher levels in J3T-1 cells, which exhibit angiogenesis-dependent invasion in the rat brain. While annexin A2 has been shown to mediate a wide variety of biological effects, to date, its functional role in glioma remains unknown [5]. In this study, the role of annexin A2 as an invasion and angiogenesis factor in malignant glioma was investigated.

## Materials and methods

### Glioma cell lines

Two cell lines, J3T-1 and J3T-2, were developed from the J3T parental canine glioma cell line, as previously described [3]. J3T-1 and J3T-2 cells were seeded in tissue culture dishes (BD Falcon, Franklin Lakes, NJ) and cultured in Dulbecco's modified Eagle's medium (DMEM) supplemented with 10 % fetal bovine serum (FBS), penicillin (100 U/ml) and streptomycin (0.1 mg/ml) [2–4, 6].

### Establishment of cell lines with targeted downregulation or overexpression of annexin A2

Targeted downregulation of annexin A2 in J3T-1 cells (J3T-1shA) was achieved by transfection of an shRNA-targeting annexin A2 (CAAGGGGACTCGTGATAAATA GTGCTCCTGGTTGTTTATCTCGAGTCCCCTTG) encoding plasmid (RNAi-Ready pSIREN-RetroQ-ZsGreen vector, Takara Bio Inc., Shiga, Japan) using TransIT-LT1 reagent (Takara Bio Inc., Shiga, Japan), according to the manufacturer's instructions. The annexin A2-overexpressing J3T-2 cell line (J3T-2A) was established by transfection of J3T-2 cells with an annexin A2-encoding plasmid (pIRES-EGFP vector, Clontech Inc., CA). For each of these cell lines, single-cell clones were selected for experiments. Cells were cultured in DMEM supplemented with 10 % FBS, penicillin (100 U/ml) and streptomycin (0.1 mg/ml) in a standard tissue incubator at 37 °C with a 5 % $CO_2$ atmosphere.

### Cell surface immunofluorescence assay

J3T-1, J3T-1shA, J3T-2 and J3T-2A cells were seeded into four-chamber, polystyrene vessel, tissue culture-treated glass slides (BD Falcon, Franklin Lakes, NJ) and incubated overnight. For immunofluorescence, cells were fixed in 4 % paraformaldehyde in phosphate-buffered saline (PBS) for 15 min. Following fixation, cells were rinsed three times with PBS. Non-specific binding was blocked by incubation in blocking buffer containing 2 % bovine serum albumin in PBS for 30 min at room temperature. Cells were then incubated overnight at 4 °C with a mouse monoclonal anti-annexin A2 antibody (1:20, Zymed Laboratories, San Francisco, CA) or mouse monoclonal anti-canine vascular endothelial growth factor (VEGF) antibody (1:20, R&D SYSTEMS, Minneapolis, MN) diluted in blocking buffer. Cells were washed three times in blocking buffer for 5 min before incubation with a secondary anti-mouse Cy3-conjugated antibody (1:300, Jackson ImmunoResearch Laboratories, Inc., West Grove, PA) for 2 h at room temperature in the dark. After three washes in PBS, the cells were counterstained with 4′,6-diamino-2-phenylindole (DAPI; 1:500, 100 ng/ml, Invitrogen, Carlsbad, CA) for 20 min at room temperature. The slides were washed three times in PBS and mounted.

### Quantitative reverse-transcription polymerase chain reaction (qRT-PCR)

Total RNA was isolated from cultured J3T-1, J3T-1shA, J3T-2 and J3T-2A cells using an RNeasy® Mini Kit (QIAGEN, Hilden, Germany) and reverse-transcribed with oligo dT primers using SuperScript III First-Strand Synthesis System for RT-PCR (Invitrogen, Carlsbad, CA), according to manufacturer's instructions. Target gene-specific primers were designed using Primer 3 Software (http://www.bioinformatics.nl/cgi-bin/primer3plus/primer3 plus.cgi) and synthesized by Invitrogen. The resulting cDNA was amplified by PCR using gene-specific primers and the 7300 Real Time PCR system (Applied Biosystems, Foster City, CA) and QuantiTect™ SYBR® Green PCR kit reagents (QIAGEN). A log-linear relationship between the amplification curve and quantity of cDNA in the range of 1–1000 copies was observed. Quantification was performed by the Comparative Ct method using 7300 Real Time PCR System with Sequence Detection Software version 1.4 (Applied Biosystems, Foster City, CA). The amount of cDNA in each sample was normalized to the crossing point of the housekeeping gene, $\beta$-actin. The following thermal

cycling parameters were used: denaturation at 95 °C for 10 min, followed by 45 cycles of 15 s at 94 °C, 30 s at 55 °C and 30 s at 72 °C. The relative expression for each gene in J3T-2 cells was calculated using their respective crossing points according to the following formula:

$$F = 2^{(TH - TG) - (OH - OG)}$$

where $F$ fold difference, $T$ J3T-2 cells, $O$ each cells, $H$ housekeeping gene ($\beta$-actin) and $G$ gene of interest.

Canine $\beta$-actin primers were $\beta$-actin F (forward), 5-GG CATCCTGACCCTGAAGTA-3 and $\beta$-actin R (reverse), 5-ACGTACATGGTTGGGGTGTT-3. Canine annexin A2 primers were annexin A2 F (forward), 5-CAGAGGATGG GTCTGTCATCG-3 and annexin A2 R (reverse), 5-CCCT TGGTGTCTTGCTGGAT-3. Canine hypoxia-inducible factor-1 (HIF-1) primers were HIF-1 F (forward), 5-TGCT CATCAGTTGCCACTTC-3 and HIF-1 R (reverse), 5-CC ATCCAGGGCTTTCAAATA-3. Canine VEGF primers were VEGF F (forward), 5-CTACCTCCACCATGCCAAG T-3 and VEGF R (reverse), 5-GCAGGATGGCTTGAA-GATGT-3. Canine platelet-derived growth factor (PDGF) primers were PDGF F (forward), GCCCGTTCAGGTGA-GAAAAA and PDGF R (reverse), 5-GTGCTTGAACTTC CGGTGCT [7].

Cell adhesion assays

A confluent monolayer of human umbilical venous cord endothelial cells (HUVECs) was incubated overnight at 37 °C in 24-well cell culture plates prior to performing cell adhesion assays. Cultured tumor cells (J3T-1, J3T-1shA, J3T-2, J3T-2A) were trypsinized with a 0.02 % EDTA and 0.05 % trypsin solution and resuspended at a concentration of $1 \times 10^7$ cells/ml in DMEM supplemented with 10 % FBS. Tumor cells were labeled by incubation with DiIC12(3) Fluorescent Dye BD$^{TM}$ (10 μg/ml, BD Biosciences, Franklin Lakes, NJ) at 37 °C for 1 h. Cells were subsequently washed to remove excess DiIC12 and resuspended at a concentration of $2 \times 10^5$ cells/ml. The cell suspension (1 ml) was placed on the HUVEC monolayer in 24-well cell culture plates and incubated for 20, 40 and 60 min at 37 °C. Non-adherent cells were removed by aspiration and a gentle rinse with PBS. Adherent, labeled tumor cells count/low power fields (LPFs) were measured in each well by fluorescence microscopy [8].

Animal glioma xenograft models

All experimental animals were housed and handled in accordance with the guidelines of the Okayama University Animal Research Committee. Prior to implantation, sub-confluent (85–90 %) J3T-1, J3T-1shA, J3T-2 and J3T-2A cells were trypsinized, rinsed with DMEM supplemented

with 10 % FBS, and centrifuged at $100 \times g$ for 5 min. The resulting cell pellet was then resuspended in PBS, and the cell concentration was adjusted to $2.0 \times 10^5$ cells/μL. Athymic rats (F344/N-nu/nu; CLEA Japan, Inc., Tokyo, Japan) were injected with 5 μL of each tumor cell suspension. Animals were anesthetized following intraperitoneal injection of nembutal (30 mg/kg) and placed in stereotactic frames (Narishige, Tokyo, Japan) with their skulls exposed. Tumor cells were injected with a Hamilton syringe (Hamilton, Reno, NV) into the right frontal lobe (4 mm lateral and 1 mm posterior to the bregma at a depth of 4 mm), and the syringe was slowly withdrawn after 5 min to prevent reflux [9]. The skulls were then cleaned, the holes sealed with bone wax, and the incision was sutured.

Histopathological analysis of glioma in rats

For histopathological analysis, athymic rats harboring brain tumors were killed 35 days after tumor implantation. Prior to killing, for immunohistochemistry and hematoxylin and eosin (HE) staining, athymic rats were anesthetized, euthanized by cardiac puncture, perfused with PBS (100 ml) and fixed with 4 % paraformaldehyde (200 ml). Brains were removed and stored in 4 % paraformaldehyde for at least 24 h. For HE staining, sections were immersed in hematoxylin for 1 min and rinsed with tap water. Sections were then immersed in eosin stain for 1–2 min and rinsed with tap water. For immunofluorescent staining, snap-frozen tissue samples were embedded in a compound of optimal cutting temperature for cryosectioning, and 20-μm cryostat sections were processed for indirect immunofluorescence. Slides were blocked with 10 % horse serum in PBS at room temperature for 60 min, and incubated overnight at 4 °C with either a mouse monoclonal anti-RECA-1 antibody (1:20, Abcam, Cambridge, MA) or a mouse monoclonal anti-annexin A2 antibody (1:20, Zymed Laboratories), diluted in 1 % horse serum in PBS. After three washes with PBS for 5 min, slides were incubated with a Cy3-conjugated anti-mouse antibody and DAPI (1:500) in PBS for 60 min. Slides were then washed in PBS and mounted. Sections were examined by fluorescence microscopy. Microvessel diameter and microvascular density was measured in 5-week-old brain tumors to assess angiogenic activity in these models (J3T-1, $n = 3$; J3T-1shA, $n = 3$; J3T-2, $n = 3$; J3T-2A, $n = 3$). For samples stained for RECA-1, five digital images were obtained (200×, 0.15 mm$^2$) from areas at the tumor borders and in the contralateral normal basal ganglia. Image J software (http://rsb.info.nih.gov/ij) was used to measure the diameter of vessels in these images. For double immunofluorescent staining, sections were incubated at room temperature for 1 h with a mouse monoclonal anti-annexin

A2 antibody (Invitrogen, 1:25) and rabbit polyclonal anti-CD31 antibody (Abcam, Boston, MA, 1:50) or rabbit polyclonal anti-α-SMA antibody (Abcam, 1:50) diluted in PBS containing 0.5 % skimmed milk. After three washes with PBS with 0.01 % Tween-20 for 5 min, sections were incubated with Alexa Fluor 594 or 488-conjugated secondary antibody (Invitrogen) in PBS for 60 min. Slides were then washed in PBS and observed.

## Immunohistochemical analysis of human glioblastoma specimens

Human glioma samples were intraoperatively obtained from patients undergoing surgical removal of tumors for diagnostic and therapeutic purposes (Okayama University Hospital, Okayama, Japan). Written, informed consent was obtained from all patients prior to surgery. Lobectomies were performed to remove the entire tumor and any surrounding brain parenchyma beyond the boundaries of the tumors observed on MRI. Glioma specimens were diagnosed and graded according to the World Health Organization classification of tumors of the central nervous system, with all 30 specimens diagnosed as glioblastomas. No patient had received radiation or chemotherapy prior to surgery. For immunohistochemical staining, sections were first deparaffinized in xylene and rehydrated in decreasing concentrations of ethanol. Sections (4 μm) were incubated in 0.3 % $H_2O_2$ for 30 min and autoclaved for 10 min at 121 °C in distilled water. After washing three times in PBS, sections were incubated at room temperature for 1 h with a mouse monoclonal anti-annexin A2 antibody (1:20, Zymed Laboratories), mouse monoclonal anti-VEGF antibody (1:100, Abcam, Boston, MA), rabbit polyclonal anti-PDGF antibody (1:100, DBS, Pleasanton, CA) or mouse monoclonal anti-HIF-1a antibody (1:20, Abcam, Boston, MA) diluted in PBS containing 5 % skimmed milk. The Dako Cytomation Envision+ System-HRP Kit was then applied according to the manufacturer's protocol (DakoCytomation, Carpintaria, CA). After three washes in PBS, sections were counterstained with hematoxylin. For immunofluorescent staining, sections were incubated at room temperature for 1 h with a mouse monoclonal anti-annexin A2 antibody (Invitrogen, 1:25), rabbit polyclonal anti-CD31 antibody (Abcam, Boston, MA, 1:50), rabbit polyclonal anti-α-SMA antibody (Abcam, 1:50) diluted in PBS containing 0.5 % skimmed milk. After three washes with PBS with 0.01 % Tween-20 for 5 min, sections were incubated with Alexa Fluor 594 or 488-conjugated secondary antibody (Invitrogen) in PBS for 60 min. Slides were then washed in PBS and observed. Expression of annexin A2, VEGF, PDGF and HIF-1α was scored qualitatively as follows: negative, no staining; weakly positive, weak to moderate, diffuse staining or sparse, intensive staining; and strong, diffuse staining. This classification was made by two neurosurgeons (M.O., J. I.) without prior knowledge of clinical or radiological patient data.

## Statistical analysis

Student's $t$ test was used to test for statistical significance. Statistical significance of vessel diameter was examined using the Mann–Whitney $U$ test. A $P < 0.05$ was considered to be statistically significant in both cases. Data are presented as the mean ± standard error. Statistical analysis was performed using Stat View statistical software (version 5.0; SAS Institute Inc., Cary, NC).

# Results

## Immunohistochemical analysis of annexin A2 and VEGF in canine glioma cell lines

Immunofluorescence assays were performed to determine the expression of annexin A2 and VEGF in J3T-1, J3T-1shA, J3T-2 and J3T-2A cells. We observed stronger expression of annexin A2 in J3T-1 and J3T-2A cells compared with J3T-2 and J3T-1shA cells (Fig. 1a–d). Similarly, the expression of VEGF was markedly higher in J3T-1 and J3T-2A cells than J3T-2 and J3T-1shA cells (Fig. 1e–h).

## qRT-PCR

We next examined the levels of *annexin A2* (Fig. 2a), *VEGF* (Fig. 2b), *PDGF* (Fig. 2c) and *HIF-1* (Fig. 2d) mRNA in J3T-1, J3T-1shA, J3T-2 and J3T-2A cells compared with J3T-2 cells by qRT-PCR. *Annexin A2* expression was significantly higher in J3T-1 and J3T-2A cells compared with J3T-2 and J3T-1shA cells (10.0-fold and 3.3-fold vs 1.0-fold and 1.6-fold, respectively, $P < 0.05$). Targeted silencing of annexin A2 in J3T-1 cells by shRNA (J3T-1shA cells) led to an 84.3 % decrease in annexin A2 expression compared with parental cells. Conversely, transfection of J3T-2 cells with a cDNA encoding annexin A2 (J3T-2A cells) led to a 232 % increase in annexin A2 expression compared with their parental counterpart. The relative expression of VEGF and PDGF was significantly higher in J3T-1 and J3T-2A cells compared with J3T-1shA and J3T-2 cells (VEGF: 7.6-fold and 15.2-fold vs 1.2-fold and 1.0-fold, respectively, PDGF: 41.7-fold and 25.7-fold vs 3.0-fold and 1.0-fold, respectively, $P < 0.05$). In contrast, we observed no significant difference in the relative expression of HIF-1a in J3T-1 and J3T-2A cells compared with J3T-1shA and J3T-2 cells (1.7-fold and 1.1-fold vs 1.2-fold and 1.0-fold, respectively).
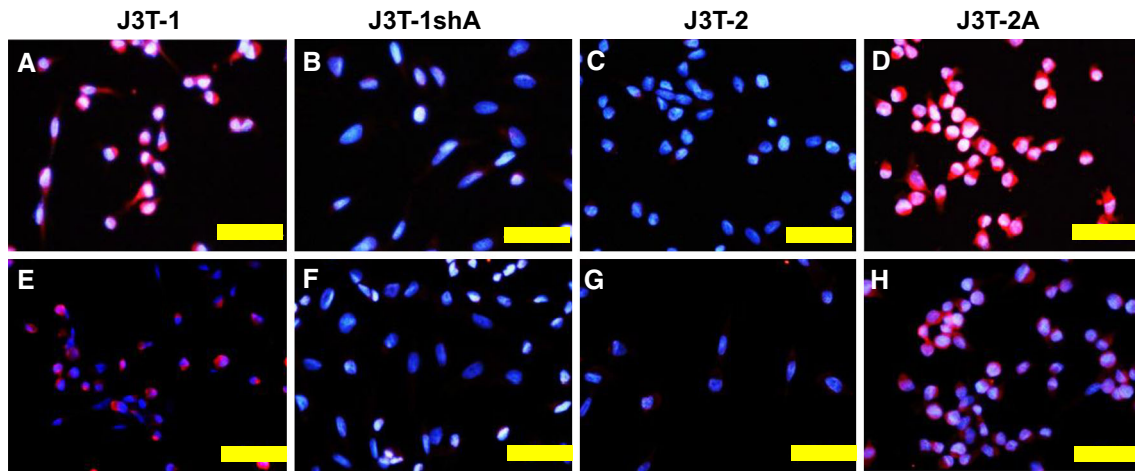
**Fig. 1** Immunohistochemical analysis of annexin A2 and VEGF expression in cultured glioma cells. The expression of annexin A2 (*red*) in J3T-1 cells (**a**) and J3T-2A cells (**d**) was significantly stronger than in J3T-1shA cells (**b**) and J3T-2 cells (**c**). The expression of VEGF (*red*) in J3T-1 cells (**e**) and J3T-2A cells (**h**) was higher than in J3T-1shA cells (**f**) and J3T-2 cells (**g**) (*scale bar* 50 μm, *blue* DAPI) (color figure online)

**Fig. 2** Analysis of *annexin A2*, *VEGF*, *PDGF* and *HIF-1* mRNA expression in cultured glioma cells. *Annexin A2*, *VEGF*, *PDGF* and *HIF-1* mRNA levels were assessed by quantitative reverse-transcription polymerase chain reaction (qRT-PCR). The relative expression of *annexin A2* (**a**), *VEGF* (**b**) and *PDGF* (**c**) was significantly higher in J3T-1 and J3T-2A cells compared with J3T-1shA and J3T-2 cells (*$P < 0.05$). *HIF-1* (**d**) levels were not significantly different between these cell lines (J3T-1 and J3T-1shA: $P = 0.262$, J3T-1 and J3T-2: $P = 0.378$, J3T-2 and J3T-2A: $P = 0.872$)
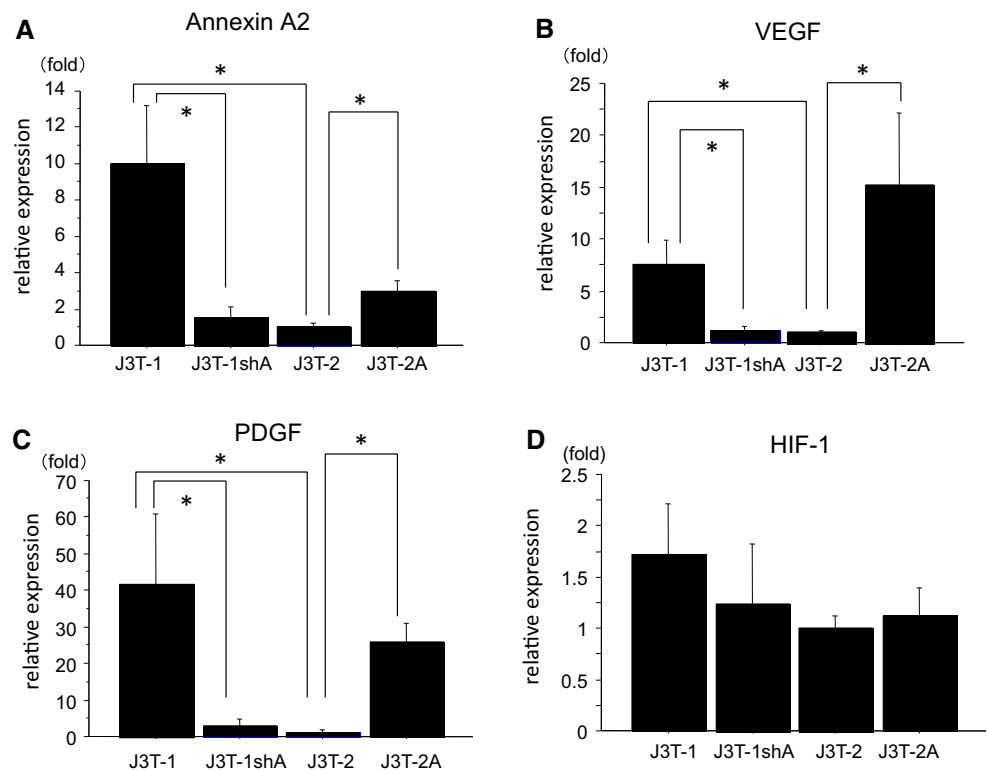


## Adhesion assays

We next investigated the effect of modulating annexin A2 expression on cell adhesion. Adhesion of J3T-1 and J3T-2A cells to HUVEC monolayers was significantly higher compared with J3T-1shA and J3T-2 cells (Fig. 3a–d). Analysis of adherent glioma cells per LPF after 1 h re-vealed that J3T-1shA cells exhibited significantly reduced adhesive ability to HUVECs compared with J3T-1 cells (Fig. 3e, $6.8 \times 10 \pm 4.8$ vs $1.4 \times 10^2 \pm 1.1 \times 10$ cells/LPF, $P < 0.05$). In contrast, J3T-2A cells exhibited significantly increased adhesion to HUVECs compared with parental J3T-2 cells ($1.81 \times 10^2 \pm 1.6 \times 10$ vs $4.0 \times 10 \pm 5.4$ cells/LPF, $P < 0.05$).

Fig. 3 Adhesive ability of glioma cells to HUVECs. Fluorescence microscopy of DiIC12-labeled tumor cells revealed that adhesion of J3T-1 cells (a) and J3T-2A cells (d) to HUVEC monolayers was significantly higher compared with J3T-1shA cells (b) and J3T-2 cells (c) (*P < 0.05). The number of adherent glioma cells per low power field (LPF) was as follows; J3T-1: $1.44 \times 10^2 \pm 1.1 \times 10$ cells/LPF, J3T-1shA: $6.76 \times 10 \pm 4.8$ cells/LPF, J3T-2; $4.0 \times 10 \pm 5.4$ cells/LPF, J3T-2A; $1.81 \times 10^2 \pm 1.6 \times 10$ cells/LPF (e)
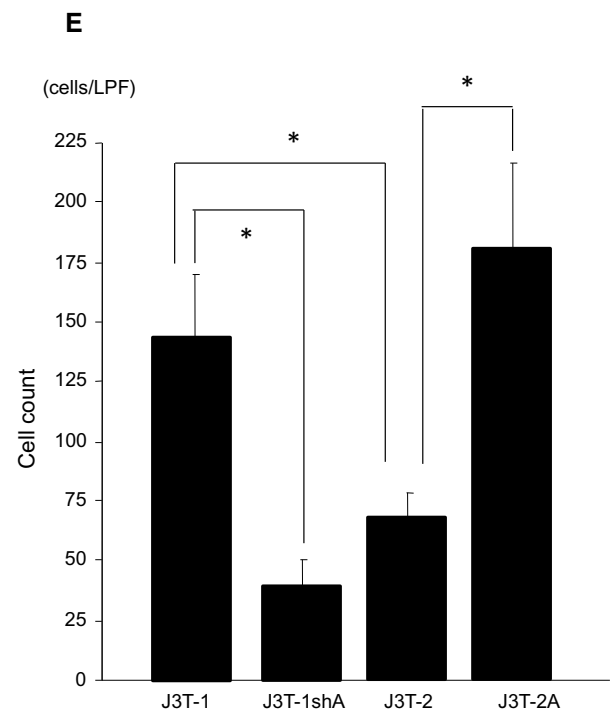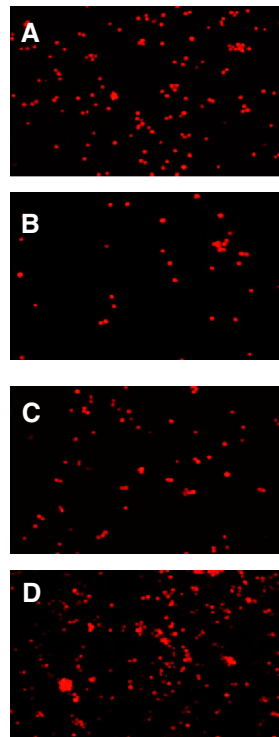


## Immunohistochemical analysis of annexin A2 expression in animal glioma models

To confirm silencing or overexpression of annexin A2 in vivo, immunohistochemical staining was also performed in brain sections of animals harboring either J3T-1, J3T-1shA, J3T-2 or J3T-2A brain tumors (Fig. 4). Intense staining of annexin A2 was observed in J3T-1 (Fig. 4a) and J3T-2A (Fig. 4d) tumor cells, whereas expression was almost undetectable in J3T-1shA (Fig. 4b) and J3T-2 tumor cells (Fig. 4c).

## Invasive phenotypes in animal brains

Athymic rats inoculated with J3T-1, J3T-1shA, J3T-2 or J3T-2A cells developed brain tumors after 28 days. J3T-1 cells formed well-demarcated, highly angiogenic tumors in rat brains (Fig. 4e). In normal parenchyma adjacent to the main J3T-1 tumor mass, multiple satellites of tumor cells were observed, containing dilated blood vessels (Fig. 4e inset). J3T-1 brain tumors exhibited an "angiogenesis-dependent invasion" pattern. J3T-1shA brain tumors (Fig. 4f) and J3T-2 brain tumors (Fig. 4g) exhibited similar histological patterns, forming poorly demarcated tumors. Tumor cells were observed in a gradually dispersed pattern from the tumor center to the normal brain parenchyma with a gradient of cell density, making the tumor border unclear. In normal parenchyma adjacent to the main tumor mass, single-cell infiltration into the normal brain parenchyma without angiogenesis was observed (Fig. 4f, g inset). J3T-1shA brain tumors and J3T-2 brain tumors thus exhibited an "angiogenesis-independent invasion" pattern. In contrast, the invasion border of J3T-2A brain tumors was clearer than that of J3T-2 brain tumors (Fig. 4h). In normal parenchyma adjacent to the J3T-2A main tumor mass (Fig. 4h inset), numerous, small tumor clusters surrounding blood vessels were observed. We also observed co-option and invasion of several J3T-2A cells to blood vessels, in addition to infiltration of single J3T-2A cells into normal brain parenchyma. While J3T-2A cells exhibited an "angiogenesis-independent invasion" pattern, they demonstrated a more "angiogenesis-dependent invasion" phenotype compared with parental J3T-2 cells.

## Angiogenesis in brain tumors

To characterize the neovasculature of J3T-1 brain tumors, brain sections were stained with annexin A2 and CD31, an endothelial marker, or α-SMA, a pericyte marker (Fig. 5). J3T-1 brain tumor collected from the invasive edge exhibited positive staining for annexin A2 (red) in clusters of tumor cells surrounding the dilated vessels. In dilated neovasculature, inner lining cells were positive for CD31 (Fig. 5a). Outer lining of multiple layers of cells were positive for α-SMA (Fig. 5b). Neither endothelial cells nor pericytes were positive for annexin A2 (scale bar = 50 μm).
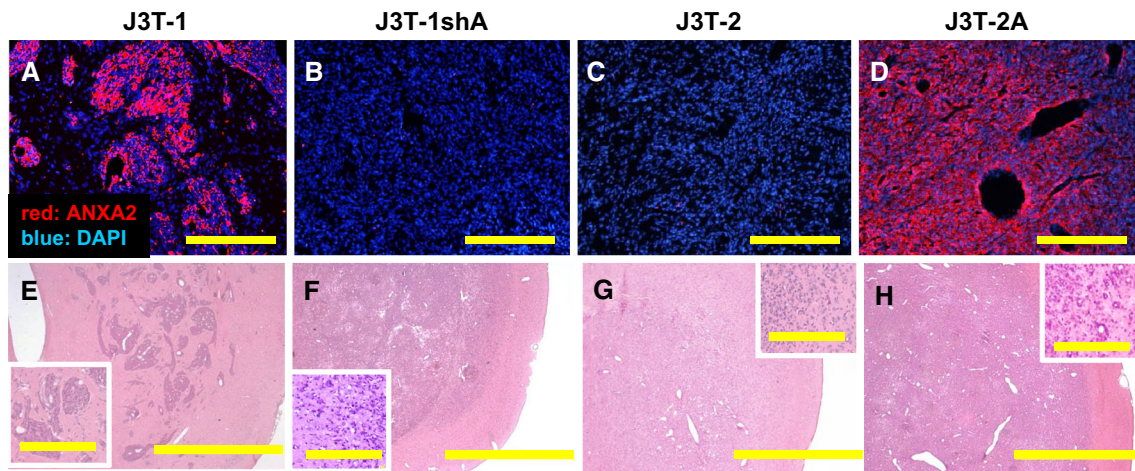
**Fig. 4** Histopathological analysis of animal glioma models. Immunohistochemical analysis of animal brain tumors revealed that J3T-1 tumors (**a**) and J3T-2A tumors (**d**) were positive for annexin A2 expression (*red*), whereas J3T-1shA tumors (**b**) and J3T-2 tumors (**c**) were negative for annexin A2 (*scale bar* 200 μm, *blue* DAPI). Macroscopic and high magnification at tumor borders (*inset*), photomicrographs of J3T-1 (**e**), J3T-1shA (**f**), J3T-2 (**g**) and J3T-2A (**h**) brain tumors in athymic rats are shown. J3T-1 cells formed well-demarcated and highly angiogenic tumors (**e**). In normal parenchyma adjacent to the main J3T-1 tumor mass, multiple satellites of tumor cells were observed, containing dilated blood vessels (**e**, *inset*). J3T-1shA brain tumors and J3T-2 brain tumors exhibited very similar histological patterns (**f**, **g**). In the tumor border area, single-cell infiltration into the normal brain parenchyma without angiogenesis was observed (**f**, **g**, *inset*). The invasion border of J3T-2A brain tumors was more distinguishable than that of J3T-2 brain tumors (**h**). In normal parenchyma adjacent to the main tumor mass, the majority of tumor cells exhibited single-cell infiltration; however, several tumor cells co-opted blood vessels (*inset, scale bar* 2 mm, 200 μm) (color figure online)
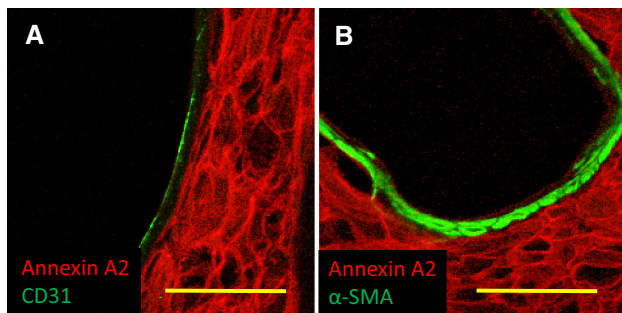


**Fig. 5** Immunehistopathological analysis of neovasculature in animal glioma models. J3T-1 brain tumor collected from the invasive edge exhibited positive staining for annexin A2 (*red*) in clusters of tumor cells surrounding the dilated vessels. In dilated neovasculature, inner lining cells were positive for CD31, an endothelial marker (**a**). Outer lining of multiple layers of cells was positive for α-SMA, a pericyte marker (**b**). Neither endothelial cells nor pericytes were positive for annexin A2 (*scale bar* 50 μm) (color figure online)

To analyze the angiogenic activity of J3T-1, J3T-1shA, J3T-2 and J3T-2A brain tumors, brain sections were stained with RECA-1 and DAPI. In J3T-1 (Fig. 6a) and J3T-2A (Fig. 6d) brain tumors, large, dilated vessels, recognized as neovascular vessels, were observed at the tumor centers. In contrast, dilated vessels were not observed at the centers of J3T-1shA (Fig. 6b) or J3T-2 (Fig. 6c) tumors. We next quantitated angiogenic activity by measuring the diameter of vessels in each brain tumor and in the contralateral normal brain area using Image J software. We observed a significant increase in the diameter of vessels in J3T-1 and J3T-2A tumors, but not in J3T-1shA and J3T-2 tumors, compared with those in contralateral normal brain tissue ($1.0 \times 10 \pm 0.6$ μm, $1.0 \times 10 \pm 0.7$ μm, $6.6 \pm 0.2$ μm, $6.2 \pm 0.1$ μm vs $3.7 \pm 0.2$ μm, respectively, *, **$P < 0.05$, Fig. 5e). Microvascular density of J3T-1, J3T-1shA, J3T-2 and J3T-2A brain tumors and normal area was $8.8 \pm 1.9$/LPF, $7.2 \pm 1.2$/LPF, $7.4 \pm 1.9$/LPF, $9.6 \pm 1.9$/LPF, $2.4 \pm 1.4$/LPF, respectively. There was no statistic difference in microvascular density of J3T-1, J3T-1shA, J3T-2 and J3T-2A brain tumors (Fig. 6f).

**Immunohistochemical analyses of annexin A2, VEGF, PDGF and HIF-1α expression in human glioblastoma samples**

Immunohistochemical analyses of glioblastoma specimens collected from the invasive edge of tumors revealed positive expression of annexin A2 in the clusters of tumor cells around the dilated vessels (Fig. 7a). The majority of human glioblastoma cases were positive for annexin A2 expression (25/30 cases), with 11/30 cases strongly positive, 14/30 cases weakly positive and the remaining five cases negative. Clusters of tumor cells surrounding the dilated vessels were also positive for VEGF (Fig. 7b), PDGF (Fig. 7c) and HIF-1 (Fig. 7d) expression. Multiple layers of vessel cells were also positive for PDGF (Fig. 7c) and HIF-1 (Fig. 7d), while only the lining cells of the vessels were

**Fig. 6** Angiogenic activity of animal brain tumors. To analyze the angiogenic activity of J3T-1, J3T-1shA, J3T-2 and J3T-2A brain tumors, brain sections were stained with RECA-1 (*red*) and DAPI (*blue*). High angiogenic activity and numerous dilated vessels were present at the center of J3T-1 (**a**) and J3T-2A (**d**) tumors. No dilated vessels were present in J3T-1shA and J3T-2 tumors (**b**, **c**). Vessel diameter was significantly increased in J3T-1 and J3T-2A tumors but not in J3T-1shA and J3T-2 tumors, compared with contralateral normal brain (**e**) (*J3T-1, J3T-2A: $P < 0.05$, J3T-1shA: $P = 0.9626$, J3T-2: $P = 0.3632$) (*scale bar* 200 μm). There was no difference in microvascular density of J3T-1, J3T-1shA, J3T-2 and J3T-2A brain tumors (**f**) (color figure online)
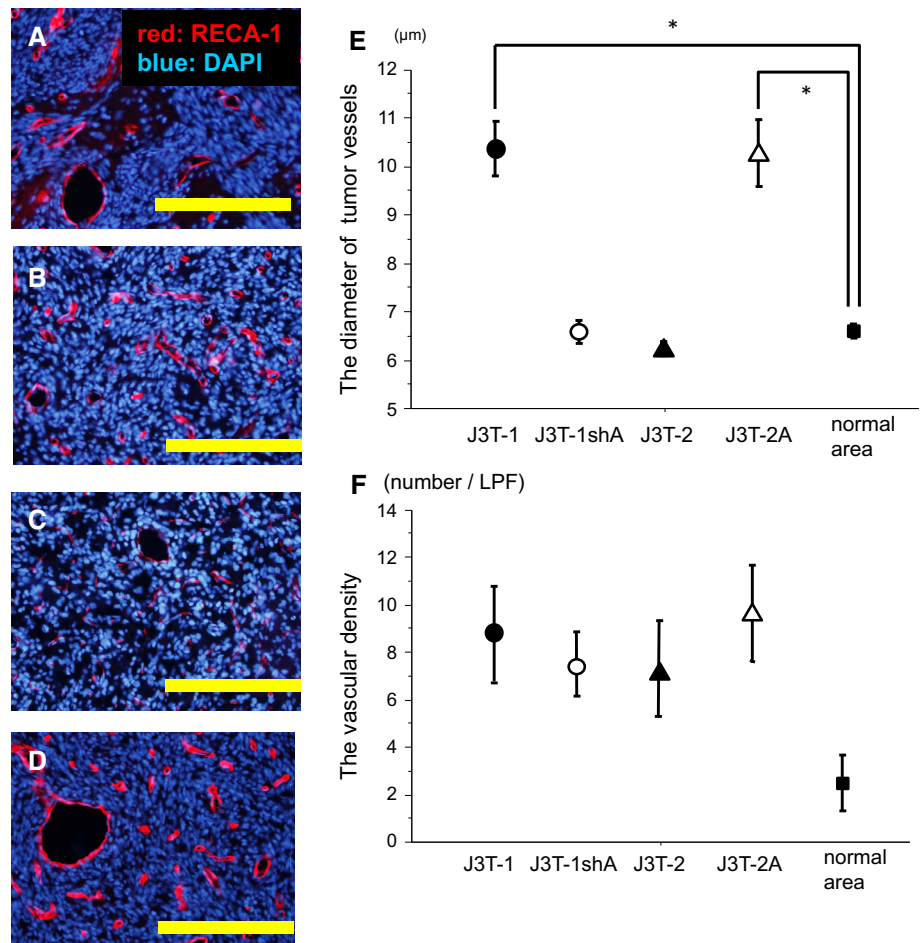


positive for annexin A2 (Fig. 7a) and VEGF (Fig. 7b). Double staining for annexin A2 (red) and CD31 (endothelial marker) (Fig. 7e) or α-SMA (pericyte marker) (Fig. 7f) revealed annexin A2 was positive in lining cells which were positive for CD31 but negative in pericyte (scale bar = 100 μm).

The expression of annexin A2, VEGF, PDGF and HIF-1α was next qualitatively scored and compared. We observed a positive correlation between annexin A2 expression and VEGF (Fig. 8a) and PDGF (Fig. 8b) staining (Annexin A2/VEGF: $R = 0.73$, $P < 0.05$, Annexin A2/PDGF; $R = 0.37$, $P < 0.05$). In contrast, no correlation was observed between annexin A2 and HIF-1α expression (data not shown).

## Discussion

Annexin A2 is a member of the annexin superfamily of $Ca^{2+}$-dependent phospholipid-binding proteins which are expressed in most eukaryotic cell types, with 12 members found in vertebrates (anx1–anx11, anx13) [10]. Increased expression of annexin A2 has been described in several tumor types, including gastric carcinoma [11], colorectal cancer [12], pancreatic cancer [13], breast cancer [14], kidney cancer [15], vascular tumors [16] and high-grade gliomas [17]. In gliomas, annexin A2 expression is observed more frequently in high-grade glioma than low-grade glioma [18, 19], and was proposed to serve as a histological marker for high-grade gliomas [17]. In our study, the majority of human glioblastoma cases (25/30 cases) were positive for annexin A2 expression. Previous studies indicate that annexin A2 mediates a wide variety of biological effects. Recent evidence suggests that annexin A2 plays an important role in neovascularization, by promoting the degradation of extracellular matrix, vascular endothelial cell migration and vascular remodeling [20, 21]. However, despite numerous studies, the functional role of annexin A2 in gliomas remains unclear [5]. In this study, the function of annexin A2 in malignant glioma in relation to angiogenesis and invasion was investigated by regulating annexin A2 expression using novel animal models. We showed that annexin A2 has at least two major functions in malignant glioma: first to mediate adhesion of glioma cells
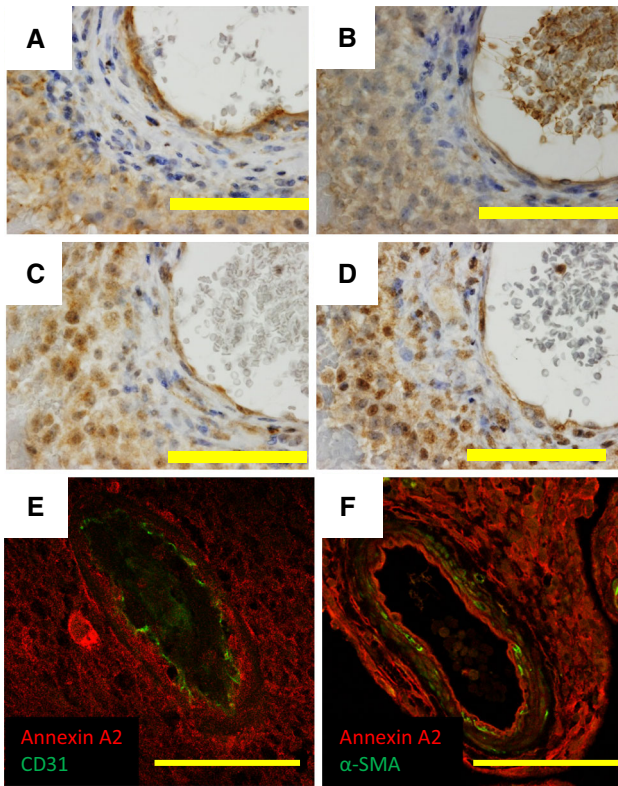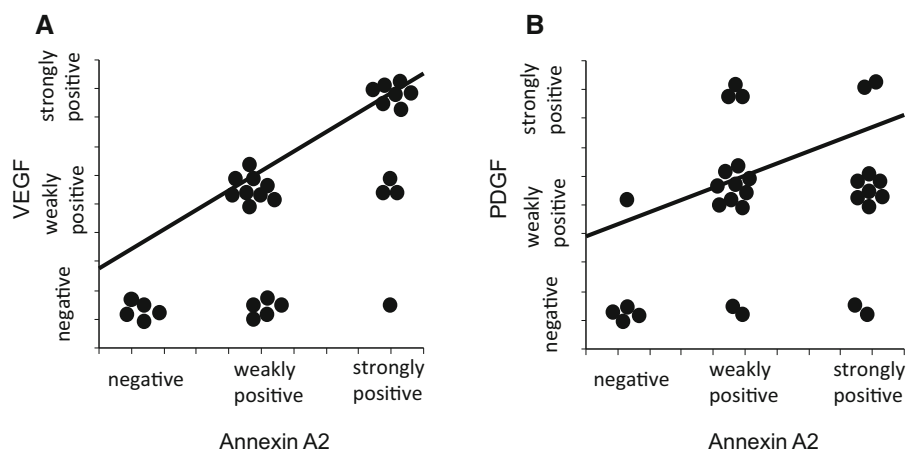
**Fig. 7** Immunohistochemical staining for annexin A2, VEGF, PDGF and HIF-1α in human glioblastoma specimens. Glioblastoma specimens collected from the invasive edge exhibited positive staining for annexin A2 (**a**), VEGF (**b**) and PDGF (**c**), in clusters of tumor cells surrounding the dilated vessels. Multiple layers of vessel cells were also positive for PDGF (**c**) and HIF-1 (**d**) while only the lining cells of the vessels were positive for annexin A2 (**a**) and VEGF (**b**). Diffuse, positive staining for HIF-1α was observed in tumor cells (**d**). Double staining for annexin A2 (*red*) and CD31 (endothelial marker) (**e**) or α-SMA (pericyte marker) (**f**) revealed annexin A2 was strongly positive in tumor cells surrounding dilated vessels and lining cells which were positive for CD31 and weakly positive in pericyte (*scale bar* 100 μm) (color figure online)

to vascular endothelial cells, and second to induce angiogenesis by promoting angiogenic factors in glioma cells.

First, we demonstrate that annexin A2 induces vascular co-option of tumor cells. Adhesion of J3T-1 and J3T-2A cells to HUVEC monolayers was significantly higher compared with J3T-1shA and J3T-2 cells. In human glioblastoma specimens, annexin A2 expression was positive in clusters of tumor cells surrounding the dilated vessels. These results suggest that expression of annexin A2 may promote glioma cell binding to endothelial cells. These results are strengthened by findings from Tressler et al., where annexin A2 was prominently expressed on the external surface of a lymphoma cell line, and mediated adhesion of these lymphoma cells to hepatic sinusoid endothelial cells [22]. Jung et al. [23] also reported that annexin A2 regulates hematopoietic stem cell homing and binding to bone marrow microenvironmental niches, including vascular and endosteal niches.

Second, we also demonstrate that annexin A2 regulates angiogenesis. The expression of annexin A2, VEGF and PDGF was higher in J3T-1 and J3T-2A cells compared with J3T-1shA and J3T-2 cells. The intensity of VEGF and PDGF staining positively correlated to annexin A2 expression in human glioblastoma specimens. These results suggest that annexin A2 induces angiogenesis by promoting angiogenic factors, such as VEGF and PDGF. In previous studies, Bao et al. [24] reported that silencing of *annexin A2* by siRNA inhibited the expression of proangiogenic molecules. Zhao et al. [25] also reported that annexin A2 regulates VEGF expression through a positive feedback mechanism.

To induce "angiogenesis-dependent invasion", glioma cells first co-opt around existing cerebral blood vessels and remove astrocyte foot processes, leading to the disruption of normal contacts between endothelial cells and the



**Fig. 8** Correlation of annexin A2, VEGF, PDGF and HIF-1α expressions in human glioblastoma specimens. The majority of human glioblastoma cases were positive for annexin A2 (25/30 cases). The intensity of VEGF (**a**) and PDGF (**b**) staining correlated with the expression of annexin A2 (correlation coefficient: annexin A2/VEGF; $R = 0.73$, $P < 0.0001$, annexin A2/PDGF; $R = 0.37$, $P < 0.05$)

basement membrane [26]. Subsequently, angiogenesis progression is mediated by several angiogenic factors secreted by glioma cells, including VEGF or PDGF. J3T-1shA and J3T-2 cells were not able to establish "angiogenesis-dependent invasive" tumors, since they lacked the ability to adhere to vascular endothelial cells and to express angiogenic factors. Previous clinical reports also suggest that angiogenesis is an important factor underlying invasive phenotypes. de Groot et al. [27] reported cases of gliomas demonstrating an apparent phenotypic shift to a predominantly infiltrative pattern of tumor progression following treatment with bevacizumab, a monoclonal antibody to VEGF. Although glioma cells possess the innate ability to invade normal brain parenchyma, independently of vascular structures, they gain the ability to co-opt and migrate along the external walls of the vasculature when they express annexin A2. Therefore, expression of annexin A2 is capable of switching these two invasion phenotypes.

The transcription factor HIF-1, which is composed of two subunits, HIF-1β and HIF-1α, is the classical and most well-characterized hypoxia-regulated molecule contributing to tumor invasion and angiogenesis. *VEGF* is an example of a gene regulated by HIF-1. In our study, J3T-1, J3T-1shA, J3T-2 and J3T-2A cells did not exhibit significant differences in HIF-1α expression levels. Based on this, we conclude that changes in VEGF and PDGF expression were not affected by HIF-1, but by annexin A2 expression.

Recent studies revealed that locally proliferated pericyte was the main constituent of microvascular proliferation in high-grade glioma [28]. In our study, J3T-1, angiogenesis-dependent invasion phenotype brain tumor, showed pericyte hyperplasia around neovasculature, which was similar to that of human glioblastoma. However, there was a difference in annexin A2 expression pattern between our animal model and human glioblastoma. This might reflect difference in the mechanisms of angiogenesis. Further study is necessary for the clarification of mechanisms of angiogenesis in malignant gliomas.

In this study, we show that the expression of annexin A2 correlates with that of VEGF and PDGF. Therefore, annexin A2 may represent an important anti-angiogenesis therapeutic target in the treatment of glioma [25, 29]. Our study demonstrated that J3T-1 animal brain tumors exhibiting an "angiogenesis-dependent invasion" phenotype shift to an "angiogenesis-independent invasion" phenotype following silencing of annexin A2 in J3T-1shA brain tumors. This phenotypic shift caused by annexin A2-targeted therapy is similar to the phenomenon observed following anti-angiogenic therapy with bevacizumab [27]. Thus, concomitant therapeutic strategies employing anti-angiogenic and anti-invasive agents are necessary to control this complicated disease [4].

## Conclusions

Our results demonstrate that the phenotype of glioma invasion is closely related to angiogenesis. The level of annexin A2 controls invasion phenotypes by regulating angiogenesis and vascular co-option. Annexin A2 is one of the several factors regulating angiogenesis and invasion of malignant gliomas.

## References

1. Stupp R, Mason WP, van den Bent MJ et al (2005) Radiotherapy plus concomitant and adjuvant temozolomide for glioblastoma. N Engl J Med 352(10):987–996
2. Onishi M, Ichikawa T, Kurozumi K, Date I (2011) Angiogenesis and invasion in glioma. Brain Tumor Pathol 28(1):13–24
3. Inoue S, Ichikawa T, Kurozumi K et al (2012) Novel animal glioma models that separately exhibit two different invasive and angiogenic phenotypes of human glioblastomas. World Neurosurg 78(6):670–682
4. Maruo T, Ichikawa T, Kanzaki H et al (2013) Proteomics-based analysis of invasion-related proteins in malignant gliomas. Neuropathology 33(3):264–275
5. Tatenhorst L, Rescher U, Gerke V, Paulus W (2006) Knockdown of annexin 2 decreases migration of human glioma cells in vitro. Neuropathol Appl Neurobiol 32(3):271–277
6. Onishi M, Ichikawa T, Kurozumi K et al (2013) Bimodal anti-glioma mechanisms of cilengitide demonstrated by novel invasive glioma models. Neuropathology 33(2):162–174
7. Godiksen S, Selzer-Plon J, Pedersen ED et al (2008) Hepatocyte growth factor activator inhibitor-1 has a complex subcellular itinerary. Biochem J 413(2):251–259
8. Nakamori S, Okamoto H, Kusama T et al (1997) Increased endothelial cell retraction and tumor cell invasion by soluble factors derived from pancreatic cancer cells. Ann Surg Oncol 4(4):361–368
9. Ichikawa T, Tamiya T, Adachi Y et al (2000) In vivo efficacy and toxicity of 5-fluorocytosine/cytosine deaminase gene therapy for malignant gliomas mediated by adenovirus. Cancer Gene Ther 7(1):74–82
10. Moss SE, Morgan RO (2004) The annexins. Genome Biol 5(4):219
11. Emoto K, Sawada H, Yamada Y et al (2001) Annexin II overexpression is correlated with poor prognosis in human gastric carcinoma. Anticancer Res 21(2B):1339–1345

12. Duncan R, Carpenter B, Main LC, Telfer C, Murray GI (2008) Characterisation and protein expression profiling of annexins in colorectal cancer. Br J Cancer 98(2):426–433

13. Esposito I, Penzel R, Chaib-Harrireche M et al (2006) Tenascin C and annexin II expression in the process of pancreatic carcinogenesis. J Pathol 208(5):673–685

14. Sharma MR, Koltowski L, Ownbey RT, Tuszynski GP, Sharma MC (2006) Angiogenesis-associated protein annexin II in breast cancer: selective expression in invasive breast cancer and contribution to tumor invasion and progression. Exp Mol Pathol 81(2):146–156

15. Zimmermann U, Woenckhaus C, Pietschmann S et al (2004) Expression of annexin II in conventional renal cell carcinoma is correlated with Fuhrman grade and clinical outcome. Virchows Arch 445(4):368–374

16. Syed SP, Martin AM, Haupt HM, Arenas-Elliot CP, Brooks JJ (2007) Angiostatin receptor annexin II in vascular tumors including angiosarcoma. Hum Pathol 38(3):508–513

17. Reeves SA, Chavez-Kappel C, Davis R, Rosenblum M, Israel MA (1992) Developmental regulation of annexin II (Lipocortin 2) in human brain and expression in high grade glioma. Cancer Res 52(24):6871–6876

18. Roseman BJ, Bollen A, Hsu J, Lamborn K, Israel MA (1994) Annexin II marks astrocytic brain tumors of high histologic grade. Oncol Res 6(12):561–567

19. Iwadate Y, Sakaida T, Hiwasa T et al (2004) Molecular classification and survival prediction in human gliomas based on proteome analysis. Cancer Res 64(7):2496–2501

20. Rescher U, Gerke V (2004) Annexins–unique membrane binding proteins with diverse functions. J Cell Sci 117(Pt 13):2631–2639

21. Sharma MC, Sharma M (2007) The role of annexin II in angiogenesis and tumor progression: a potential therapeutic target. Curr Pharm Des 13(35):3568–3575

22. Tressler RJ, Updyke TV, Yeatman T, Nicolson GL (1993) Extracellular annexin II is associated with divalent cation-dependent tumor cell-endothelial cell adhesion of metastatic RAW117 large-cell lymphoma cells. J Cell Biochem 53(3):265–276

23. Jung Y, Wang J, Song J et al (2007) Annexin II expressed by osteoblasts and endothelial cells regulates stem cell adhesion, homing, and engraftment following transplantation. Blood 110(1):82–90

24. Bao H, Jiang M, Zhu M, Sheng F, Ruan J, Ruan C (2009) Overexpression of Annexin II affects the proliferation, apoptosis, invasion and production of proangiogenic factors in multiple myeloma. Int J Hematol 90(2):177–185

25. Zhao SH, Pan DY, Zhang Y, Wu JH, Liu X, Xu Y (2010) Annexin A2 promotes choroidal neovascularization by increasing vascular endothelial growth factor expression in a rat model of argon laser coagulation-induced choroidal neovascularization. Chin Med J (Engl) 123(6):713–721

26. Zagzag D, Amirnovin R, Greco MA et al (2000) Vascular apoptosis and involution in gliomas precede neovascularization: a novel concept for glioma growth and angiogenesis. Lab Invest 80(6):837–849

27. de Groot JF, Fuller G, Kumar AJ et al (2010) Tumor invasion after treatment of glioblastoma with bevacizumab: radiographic and pathologic correlation in humans and mice. Neuro Oncol 12(3):233–242

28. Sun H, Guo D, Su Y, Yu D, Wang Q et al (2014) Hyperplasia of pericytes is one of the main characteristics of microvascular architecture in malignant glioma. PLoS One 9(12):e114246

29. Kesavan K, Ratliff J, Johnson EW et al (2010) Annexin A2 is a molecular target for TM601, a peptide with tumor-targeting and anti-angiogenic effects. J Biol Chem 285(7):4366–4374